Cement & Concrete Composites 37 (2013) 222–231

Contents lists available at SciVerse ScienceDirect

Cement & Concrete Composites

journal homepage: www.elsevier.com/locate/cemconcomp

Confinement of concrete with hybrid FRP bistable structures

Christopher Quon [a], Lijuan Cheng [b,*], Yang Li [c], William Yu [d]

[a] AECOM, 2020 L St., Suite 300, Sacramento, CA 95811, USA
[b] Department of Civil and Environmental Engineering, University of California, Davis, One Shields Ave., Davis, CA 95616, USA
[c] Shanghai Municipal Engineering Design General Institute Co., 901 Zhong Shan Bei Er Rd., Shanghai 200092, PR China
[d] City of San Francisco, 1 D. Carlton B. Goodlett Place, San Francisco, CA 94102, USA

ARTICLE INFO

Article history:
Received 5 November 2011
Received in revised form 13 September 2012
Accepted 14 September 2012
Available online 4 October 2012

Keywords:
Fiber reinforced polymer
Concrete
Bistable
Confinement
Analytical modeling
Stress–strain

ABSTRACT

The ductility potential of concrete confined with fiber reinforced polymer (FRP) composites is limited by the low fracture strain and brittleness of the fiber and consequently poor energy dissipation in the system. To improve this aspect, a series of experiments were conducted to investigate the use of mechanism-based hybrid FRP bistable wraps, which consist of energy-absorbing "links" made of carbon and glass fabrics bonded together (with the main links designed as the primary load carrier and the waiting links as the secondary load carrier). The FRP bistable-confined concrete was found to have increased ductility and energy absorption with a controlled failure mode. The effect due to material type of the bistable links and core inserts was substantial in terms of load-carrying capacity and deformability. A two-step simulation method was developed for the FRP-confined concrete, where the FRP wrap was modeled with a material constitutive behavior obtained from a separate modeling step of the FRP bistable structure. A simplified bilinear model was also proposed for design purpose.

1. Introduction

Fiber reinforced polymer (FRP) composites are popular for structural concrete retrofit due to their advantages, such as high strength-to-weight ratio, corrosion resistance, and ease of application. FRP-based jacketing/wrapping has become a common concrete confinement technique used to increase the effective compressive strain of concrete for large deformability and the axial load capacity, as well as prevent the buckling of longitudinal reinforcement in concrete columns. Numerous experimental studies regarding concrete confinement with FRPs have been conducted on reinforced and unreinforced concrete under axial loads [1–4], cyclic compressive loads [5], seismic loads [6], and eccentric loads [7,8]. In addition, theoretical modeling and relevant design equations have been developed [9–13]. Research on confinement using FRP jackets applied by nonconventional techniques [14] and narrow FRP strips [15] also shows the effectiveness of this FRP-based confinement for concrete. With this confinement enhancement, concrete structure's deformability and ductility can be greatly improved, which is of particular benefit for seismic rehabilitation. However, this ductility potential is rather limited by the fiber's low fracturing strain and poor energy dissipation [16,17]. Moreover, the brittle nature of the common FRP materials, such as carbon FRP (CFRP) and glass FRP (GFRP), can cause sudden rupture of the fiber resulting in brittle failure modes in the concrete structure.

This paper considers a bistable structure that is featured by a synergistic combination of two material components complimentary in their strain limits and stiffness and arranged in different geometrical configuration (i.e., straight "main links" and curved "waiting links"). The term "bistable" means having two stable states separated by a load peak [18]. In the context of this research, the bistable behavior is provided by the failure of the main links followed by the activation of the waiting links, providing a redundant load path [18]. It has been demonstrated that considerably higher deformability can be gained with certain forms of hybrid FPR bistable structure such as carbon and Spectra® hybrids under a uniaxial tension condition [19]. In addition, the working mechanism allows the overall bistable structure to increase the amount of energy absorbed compared to the materials acting alone, resulting in a more controlled fracture and a fail–safe mechanism.

The idea of bistable structure was first introduced to the FRP-confined concrete in civil engineering by Wan et al. [20]. As illustrated in Fig. 1, the bistable structure is made of hybrid composite (unidirectional CFRP for straight main link and GFRP for curved waiting link that are stitched together) and wrapped outside cylindrical concrete members to provide additional confinement. When concrete under compressive pressure starts to expand laterally,

* Corresponding author. Tel.: +1 530 754 8030; fax: +1 530 752 7872.
E-mail addresses: cgquon@ucdavis.edu (C. Quon), dawcheng@ucdavis.edu (L. Cheng), li_y.dq1@smedi.com (Y. Li), wenyu@ucdavis.edu (W. Yu).

0958-9465/$ - see front matter © 2012 Elsevier Ltd. All rights reserved.
http://dx.doi.org/10.1016/j.cemconcomp.2012.09.002

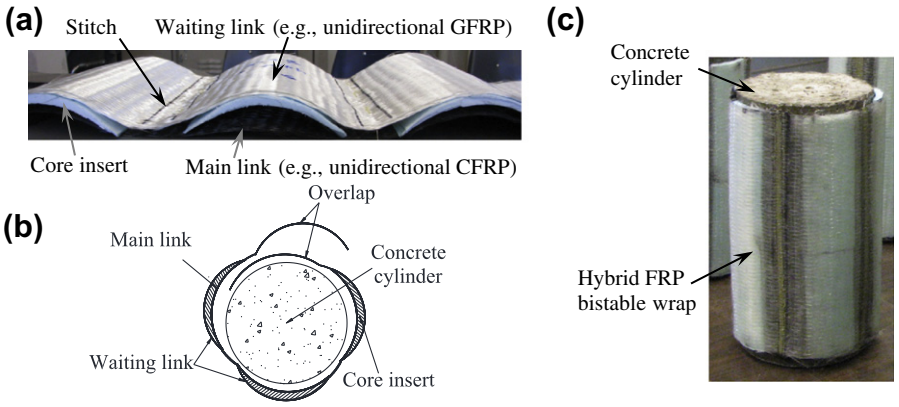

Fig. 1. Design concept: (a) hybrid FRP bistable structure, (b) bistable-confined concrete and (c) picture of a typical testing specimen.

the main link of the bistable wrap restraining the concrete undergoes tension in the hoop direction. When the first main link fractures, the corresponding waiting link is activated and continues to confine the concrete. This fracture mechanism repeats until all the main links fail and one or multiple waiting links reach the ultimate tensile capacity in the material. This proof-of-concept was explored in an earlier study [21] to examine the confinement effect due to the number of bistable segments and the size of the links. The results showed that a controlled failure with multiple signs of warning was achieved in the confined concrete. Both the member's ductility and energy absorption capacity were greatly improved. However, the load-carrying capacity of the confined structure was found to be rather limited by the quality of the bond between the FRP wrap and concrete surface due to the manually employed manufacturing process. It is also suggested in the paper that the types of FRP reinforcement and alternative materials for the foam inserts used in the bistable segments should be further investigated [21].

The objective of this research is to investigate these important parameters for more effective confinement, including the type of FRP reinforcement (GFRP vs. CFRP), core insert material type (foam, wood, rubber vs. aluminum), the amount of stitching used for sewing the links together, and alternative wrapping method. Moreover, a two-step simulation method is developed for the FRP-confined concrete where the FRP wrap was modeled with a material constitutive behavior equivalent to that from a separate modeling step of the FRP bistable structure. A theoretical bistable stress–strain model under compression is proposed based on the analytical derivation and experimental data. The results show that the proposed model can well capture the entire stress–strain behavior of the FPR bistable-confined concrete under compressive loading. A simplified bilinear model is also proposed at the end of the study for practical design purpose.

2. Experimental program

2.1. Materials and specimen

A total of thirteen sets of standard plain concrete cylinders (15.2 by 30.5 cm) were constructed in two batches. Each set contained three concrete cylinders resulting in 39 testing specimens in total (Fig. 1c). Unidirectional CFRP and GFRP laminates (both with a thickness of 1.016 mm) were used as the reinforcement for the bistable structure. The mechanical properties of these FRP materials are experimentally determined following the ASTM D3039 [22] and are summarized in Table 1 together with those for the stitching and core inserts. The tensile strength of the CFRP and GFRP laminates was obtained as 611 MPa and 520 MPa, respectively, and their corresponding Young's modulus was 54.0 GPa and 21.4 GPa. The nominal compressive strength of concrete was obtained following ASTM C39 [23] for the two batches of concrete and is provided in Table 2 where the specimens are divided into four different groups.

The first group of specimens was fabricated to study the effect of different amount of Kevlar stitches used to sew the main links (one ply of CFRP) and waiting links (two plies of GFRP) together. Stitching tends to stiffen local areas of FRP wrap in between the bistable segments that contain the crescent shaped core inserts. This can easily create voids behind the stitched area between the FRP wrap and the concrete surface and localized stress concentration. It has been found to contribute to early debonding of the FRP wrap in the previous study. The original choice of CFRP/GFRP configuration for main link/waiting link is mainly due to the consideration that the main link is expected to fail before the waiting link so that the bistable mechanism can be fully activated (i.e., a stiffer material with less ductility such as CFRP is suitable for the main link and the more flexible material with larger deformability such as GFRP for the waiting link). SP2-12M had 12 lines of Kevlar stitches, SP3-6M had 6, and SP4-0M did not have any line (only a few scattered threads to hold the foam cores in place). The bistable wrap involved had three links of a 5.5%*wait* design, which was selected based on the results from an earlier study [21]. The term "%*wait*" defines how much longer the waiting link is with respect to the length of the main link [21]. A set of baseline specimens (SP1-base) made of the same amount of reinforcement but no bistable shape was also included in this group for comparisons. These specimens were directly wrapped with one ply of CFRP (inner layer) and two plies of GFRP (outer layer). Based on the test results from the first group, a sudden load drop was observed after the first waiting link broke. This could be caused by the poor load transfer from the main link to the waiting link due to the brittleness of CFRP as the inner main link. To improve this load drop behavior, the original CFRP/GFRP configuration for main/waiting link was replaced by the reverse configuration in the second group of specimens, where less brittle GFRP was used for main link and CFRP for waiting link. SP5-1C2G had one ply of CFRP for main link and two plies of GFRP for waiting link. Oppositely, SP6-2G1C contained two plies of GFRP for main link and one ply of CFRP for waiting link.

In the third group, an alternative wrapping method called "Layer-by-Layer" (LbL) was explored in contrast with the original one piece wrapping method. So instead of fabricating the bistable structure prior to the application to concrete, the main link layers, core inserts and waiting link layers were directly wrapped onto concrete surface one at a time with epoxy resin, with no single

Table 1
Material properties.

Part	Material	Ultimate strength (MPa)	Ultimate strain (%)	Reference
Bistable links	Unidirectional CFRP/epoxy	611	1.12	ASTM D3039
	Unidirectional GFRP/epoxy	520	2.45	ASTM D3039
Stitching	Kevlar thread	3600	3.6	Manufacturer
Core	Styrofoam	1.17[a]	N/A	Manufacturer
	Douglas fir wood	75.8[b]	N/A	Manufacturer
	Neoprene rubber	6.89	N/A	Manufacturer
	Aluminum alloy 5052	227.4	N/A	Manufacturer

[a] Compressive strength for the foam only and the rest are for tensile strength.
[b] Property is for the direction parallel to the grains.

Table 2
Specimen details.

Specimen	f_c'[a] (MPa)	Main link/waiting link	Core	Wrapping method	No. of links	%*wait*[c]
1st group						
SP1-base	43.7	1CFRP + 2GFRP	None	NA[b]	NA	NA
SP2-12M	43.7	1CFRP/2GFRP	Foam	One piece with 12 lines of Kevlar stitch	3	5.5%
SP3-6M	43.7	1CFRP/2GFRP	Foam	One piece with six lines of Kevlar stitch	3	5.5%
SP4-0M	43.7	1CFRP/2GFRP	Foam	One piece with zero lines of Kevlar stitch	3	5.5%
2nd group						
SP5-1C2G	43.7	1CFRP/2GFRP	Foam	One piece with zero lines of Kevlar stitch	3	2%
SP6-2G1C	43.7	2GFRP/1CFRP	Foam	One piece with zero lines of Kevlar stitch	3	2%
SP7-1G1C	43.7	1GFRP/1CFRP	Foam	One piece with zero lines of Kevlar stitch	3	2%
3rd group						
SP8-0M	35.8	1CFRP/2GFRP	Foam	One piece with zero lines of Kevlar stitch	4	2%
SP9-LbL	35.8	1CFRP/2GFRP	Foam	Layer-by-Layer wrapping	4	2%
4th group						
SP10-foam	35.8	1CFRP/2GFRP	Foam	Layer-by-Layer wrapping	4	2%
SP11-rubber	35.8	1CFRP/2GFRP	Rubber	Layer-by-Layer wrapping	4	2%
SP12-wood	35.8	1CFRP/2GFRP	Wood	Layer-by-Layer wrapping	4	2%
SP13-alloy	35.8	1CFRP/2GFRP	Alloy	Layer-by-Layer wrapping	4	2%

[a] Average compressive strength of concrete on the day of testing per ASTM C39/C39M [23].
[b] Not applicable since the baseline specimen is wrapped in the conventional way with one ply of CFRP and two plies of GFRP with no bistable configuration.
[c] Defined as the percentage that corresponds to how much longer the waiting link is with respect to the length of the main link, i.e., %*wait* = (waiting link's length/main link's length − 1) × 100%.

stitch used. Differences are further elaborated in Section 2.2. Lastly, the effect due to different core materials was examined in the fourth group of specimens, where Styrofoam, neoprene rubber, Douglas fir wood and aluminum alloy were considered. Among these materials, foam provides the minimum amount of strength and is crushable under the circumferential expansion of the bistable links. Based on the test results from the first group of specimens, the use of foam was able to activate all the bistable links; however, it also caused a substantially large load drop after each activation of the waiting links. In order to reduce this load drop, stiffer and less crushable materials such as rubber, wood and aluminum were considered as well. All specimens in this group were fabricated using the LbL wrapping method, based on the results from the previous group. Details of all groups of test specimens are further summarized in Table 2.

2.2. Manufacturing

To prepare for the bistable wrap, unidirectional carbon and glass fabrics were first cut into the desired length and width. A spacing of 12.7 mm is reserved between the FRP wrap and the edge of the concrete cylinder on each end to prevent the direct loading of the FRP material. The crescent shaped core inserts were then created from their raw material pieces, where a hot wire cutter plus Formica templates was used for the Styrofoam (Fig. 2a) and the aluminum cores were made via a machining process. After inserting the cores between the CFRP and GFRP layers (Fig. 2b), the fabrics were stitched together along the sides of the cores using a commercial sewing machine with multiple lines of Kevlar threads (Fig. 2c and d). For the specimen set with nearly zero amount of stitches (0 M), only spotted Kevlar threads were manually sewed into the main links in order to hold the core inserts in place prior to the application of resin, in which case the strength effect due to the Kevlar stitches is negligible (not shown in Fig. 2). The typical wet lay-up process was then used to apply the prefabricated one-piece bistable wrap to concrete cylinders together with epoxy resin (Fig. 2e and f). For the alternative Layer-by-Layer wrapping method, the main and waiting links were applied one layer at a time with sufficient resin impregnation. The crescent shaped cores were attached to the cylinder after the main link but before the waiting link were wrapped. Lastly, clamps were used in the stitched areas in between the bistable segments during the curing process to minimize any void or gap caused by the stiffening effect due to the Kevlar stitches. All specimens were capped on both ends using standard sulfur capping material and were then tested under uniaxial compression via a universal testing machine in the laboratory. The total load and vertical displacement in the specimen (using linear potentiometers) were recorded through a National Instruments data acquisition system.

2.3. Testing results

2.3.1. FRP bistable wrap

To characterize the mechanical property of the FRP bistable wrap, material coupons (25.4 mm wide and 254 mm long) made of multi-link bistable structure were first prepared following

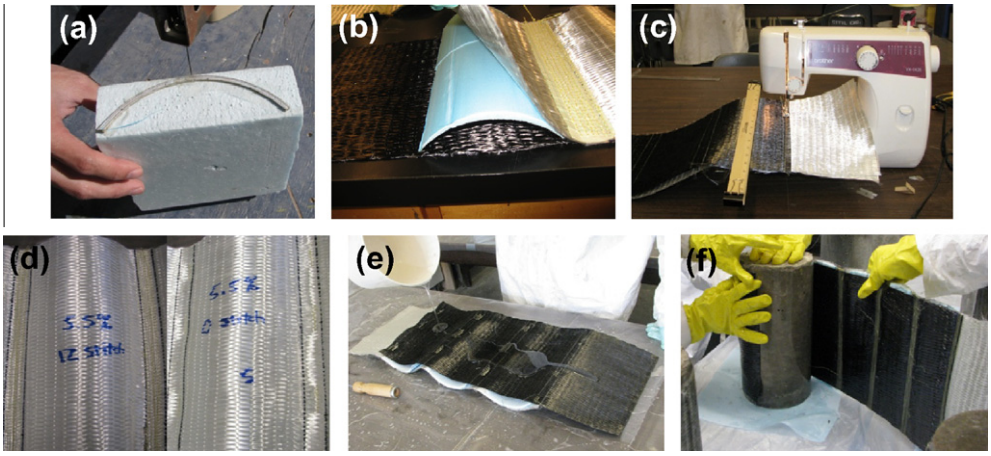

Fig. 2. Manufacturing process: (a) cutting core inserts, (b) forming bistable segment, (c) sewing, (d) finished stitching, (e) application of epoxy binder and (f) wet lay-up.

the ASTM D3039 [22] and tested under a uniaxial tension load using a MTS 810 test system. Fiberglass tabbing was applied to the specimen ends to avoid any slipping of the specimens from the machine grips. The load–displacement (or stress–strain) curve of the coupons displayed a typical bistable response, as shown in Fig. 3, where the coupons in the set were made of 3-link 5.5%*wait* bistable structure using one layer of CFRP for main link and two layers of GFRP for waiting link. The three main links ruptured sequentially each with a load drop and large deformation increase in the system. The rupture of the main links occurred mostly near the edge of the stitched areas. This local effect due to stitching likely caused the sudden load drops in the system. The final failure occurred as one of the waiting links ruptured.

2.3.2. Effect of stitching on concrete confinement

For the FRP bistable-confined concrete cylinder, the stitching was originally designed to hold the core inserts in place prior to the application to concrete and also expected to assist in transferring the load from the main link to the waiting link. However, the previous study showed that Kevlar stitches tended to stiffen the fabrics locally, causing insufficient resin impregnation and "popping out" tendency causing early debonding in that localized area [21]. In the first group of specimens, SP2-12M, SP3-6M, and SP4-0M had 12 lines, six lines, and zero lines of stitching, respectively (all with 3-link 5.5%*wait* bistable shape). It was observed that the baseline specimens (SP1-base using the same amount of FRP but conventional wrap) all failed in an explosive manner with no sign of failure. The CFRP reinforcement experienced abrupt and brittle rupture at failure. In contrast, the bistable specimens had multiple warnings in the structure prior to the final failure. At each warning, a loud popping noise was heard corresponding to the failure of a main link. Concrete further expanded with continuous confinement provided by the rest of the main links and the activated waiting links in the bistable wrap. The final failure occurred as all the main links failed and one of the waiting links reached the ultimate tensile capacity in the material. This observation was further confirmed by examining the load–displacement response of representative specimens from each set, as illustrated in Fig. 4. It can be seen that the failure mode in the bistable-confined concrete was much more progressive with substantially larger deformation, as compared to the baseline design (conventional FRP wrap). The load in SP4-0M showed three clear drops before the final failure, corresponding to the rupture of the three main links in FRP wrap. However, some of these load drops prior to failure were not that obvious in SP2-12M and SP3-6M. It can also be seen that the load-carrying capacity increased as the amount of stitching was reduced from 12 lines to zero. Since the specimens with zero lines of stitch (SP4-0M) was also able to reach similar confinement strength to the baseline design, this 0 M design was thus adopted in fabricating the next group of the testing specimens.

2.3.3. Effect of reinforcement type on concrete confinement

All specimens in the previous group utilized CFRP for the main link. The use of GFRP for the main link material was further explored in this group. Specimen sets SP5-1C2G and SP6-2G1C had exactly the same amount of reinforcement but opposite material

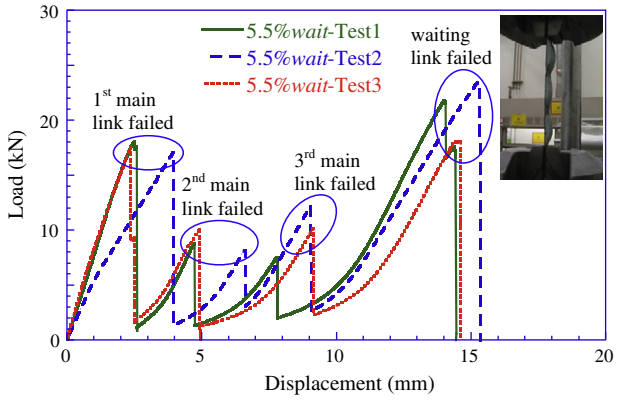

Fig. 3. Material characterization of 3-link 5.5%*wait* bistable coupons under tension.

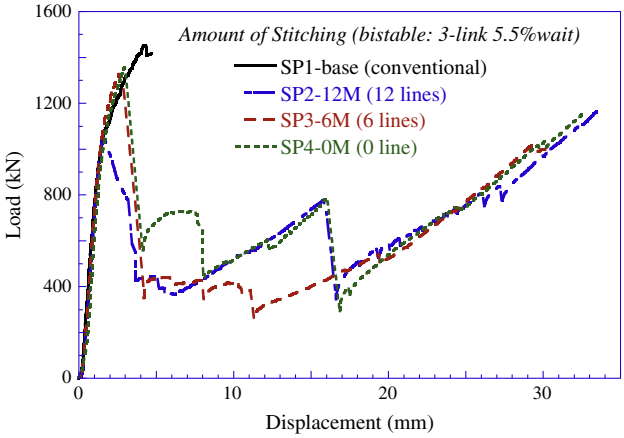

Fig. 4. Effect of stitching amount on specimen load–displacement response.

type for the main links and waiting links. It can be seen from Fig. 5 that SP5-1C2G showed a typical bistable failure as previously discussed, while SP6-2G1C did not exhibit the multi-stage breakage of the bistable links. This is mainly due to the fact that two plies of GFRP have larger deformability and tensile capacity than one ply of CFRP. Therefore the three GFRP main links broke nearly simultaneously without a bistable pattern and the CFRP waiting link continued to work until failure. As a result, the specimens had a small initial load drop and continued to resist the load till the outside CFRP waiting link ruptured. The ultimate load-carrying capacity of these two sets was close to each other, but the deformation at failure was three times smaller in SP6-2G1C than SP5-1C2G. Set SP7-1G1C (one ply of GFRP for waiting link) behaved similarly to SP6-2G1C (two plies of GFRP for waiting link) except that the load-carrying capacity at failure was about 20% lower than SP6-2G1C. It is worth of mentioning that the area under the load–displacement curve typically represents the amount of energy absorbed in the structure. This capability is often deemed beneficial for seismic design. Among the three sets of specimens, the bistable design using 1-ply CFRP for main link and 2-ply GFRP for waiting link (SP5-1C2G) showed the greatest amount of energy absorption (Fig. 5). However, the load also dropped the most during response history, which could be undesirable in the structure under certain conditions. Improvement on this load-dropping behavior was studied next.

2.3.4. Effect of wrapping method on concrete confinement

It is known that that a full contact or perfect bonding between the bistable wrap and the concrete surface is critical in ensuring an effective confinement to concrete. All specimens tested in the previous two groups were fabricated by creating the FRP bistable structure in one single piece prior to wrapping it onto the concrete cylinders. Although clamps were used during curing in the stitched regions in between the bistable segments, small voids still existed behind the stitched areas between the FRP wrap and concrete surface in many specimens. In this group, SP9-LbL was fabricated using the new Layer-by-Layer wrapping method. Fig. 6 compares the load–displacement behavior of specimens using this LbL and the original one piece-no stitch method (SP8-0M), which both showed the multi-stage failure mechanism. It can be seen that the LbL method significantly increased the load-carrying capacity of the specimens, achieving about 46% higher load capacity as compared to the set using the one piece-no stitch wrapping method. Therefore, this LbL wrapping method was adopted in manufacturing the bistable-concrete specimens in the next group.

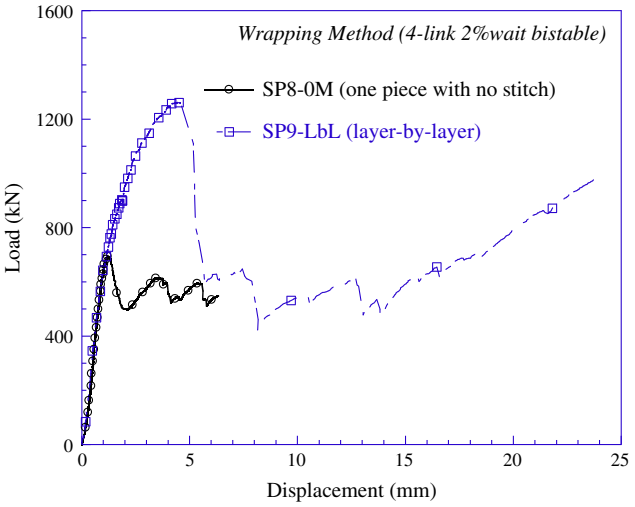

Fig. 6. Effect of wrapping method on specimen load–displacement response.

2.3.5. Effect of core material type on concrete confinement

As mentioned earlier, the bistable-confined concrete using foam core showed a large load drop when the first main link ruptured. This is likely caused by the fact that foam is a weak material and may not be able to resist stresses generated after the rupture of the main link. It thus became insufficient to transfer the load from the main link to the waiting link as the first main link breaks. Hence, stiffer materials such as rubber, wood and aluminum were considered for the core in this set of tests. Their load–displacement responses are displayed and compared in Fig. 7. It can be seen that specimens using these alternative core materials (SP11-rubber, SP12-wood and SP13-alloy) had a similar overall behavior in terms of the load-carrying capacity and displacement response. Although a load-drop was also observed after the first main link failed, this load-drop was much smaller than the original design using foam (SP10-foam). It is also noticeable that, unlike the specimens using foam core, specimens using rubber, wood and aluminum tended to only activate two bistable links rather than all before the final failure (Fig. 7). The displacements at failure were much smaller than the foam core case. Among these three alternatives, rubber core design provided the desirable amount of deformability and energy absorption in the bistable-confined concrete, thus reducing the tendency for brittle failure. Rubber core inserts remained in one piece whereas foam or wood core inserts experienced fragmentation. In addition, rubber is the most practical of the various options

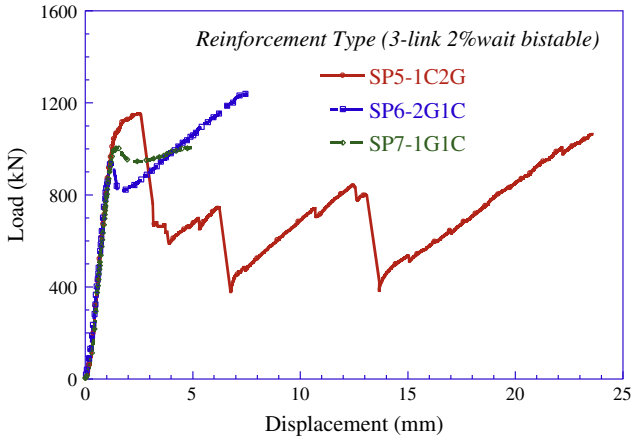

Fig. 5. Effect of reinforcement type on specimen load–displacement response.

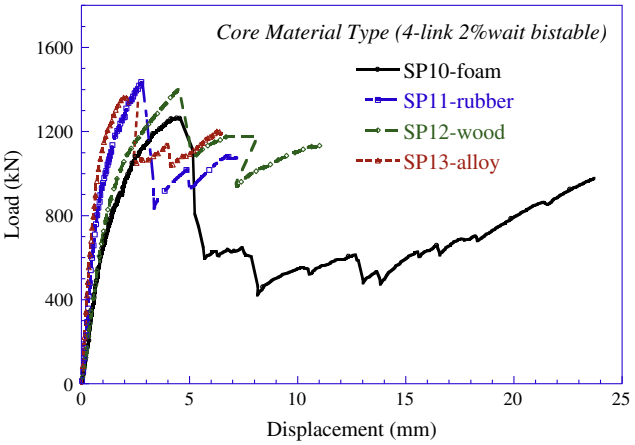

Fig. 7. Effect of core insert material type on specimen load–displacement response.

considered here. The use of aluminum would be costly and wood has other issues, such as its variability and susceptibility to some environmental exposures.

3. Modeling approach

In order to further explore the bistable design concept with a wider range of parameters, a two-step simulation method was developed using commercial finite element analysis software ANSYS [24]. During the first step, a constitutive stress–strain (load–displacement) relation was obtained for the hybrid FRP bistable wrap using the laboratory material properties. This load–displacement response was then used as the equivalent properties for the FRP wrap to analyze the FRP-confined concrete structure during the second step of the modeling.

3.1. Step I: Modeling of hybrid FRP bistable structure

The major components of a typical bistable wrap include main links, waiting links and core inserts. Shell element (Shell41) was used to model the FRP links and solid element (Solid45) was applied to the core inserts. Both elements allow for large deformability [24]; and therefore the geometric nonlinearity effect was included. All materials were assumed to be linear elastic and a perfect bond was assumed in the stitching areas. A uniformly distributed tensile pressure was applied along the edge of one end of the structure while the other end was given a fixed boundary condition (Fig. 8). Considering FRP composites are mostly linear elastic materials that fail in a brittle manner, the elements in the main links were deactivated (considered as failed elements) once their tensile stress reached the ultimate capacity of the material. The load vs. displacement response of the bistable structure was then obtained using the standard analysis procedure in ANSYS. The load–displacement response and the equivalent modulus and strength were then used in the next step as the constitutive properties for the equivalent FRP wrap outside the concrete core.

3.2. Step II: Modeling of FRP bistable-confined concrete

Importing the stress–strain (load–displacement) response from Step I as the equivalent material properties for the hybrid FRP confining wrap, a quarter model of the bistable-confined concrete cylinder was created at the beginning of this step. Shell element (Shell43) was adopted to simulate the confining wrap since it allows the user to define multilinear elastic material properties. Since all the fibers in the FRP wrap were oriented in the hoop direction of the cylinder, contribution to the compressive stiffness in the member's vertical direction is negligible. Thus, the equivalent elastic modulus of the wrap in its vertical direction was assumed to be negligibly small (e.g., 1×10^{-5} GPa). For the concrete core, solid element (Solid65) was adopted. It is typically used for three-dimensional modeling of solids with or without reinforcing bars and capable of cracking in tension and crushing in compression, which makes it suitable for modeling the quasi-brittle behavior of concrete. The constitutive model of nonlinear concrete was represented by the well-known Hognestad model [25], which approximates the stress–strain relationship of concrete by a parabola up to the ultimate strength (f_c') and a straight line beyond that up to the crushing of concrete. The confined concrete cylinder was subjected to a fixed boundary condition at the bottom and a uniformly distributed compressive pressure on the top surface (as shown in Fig. 8).

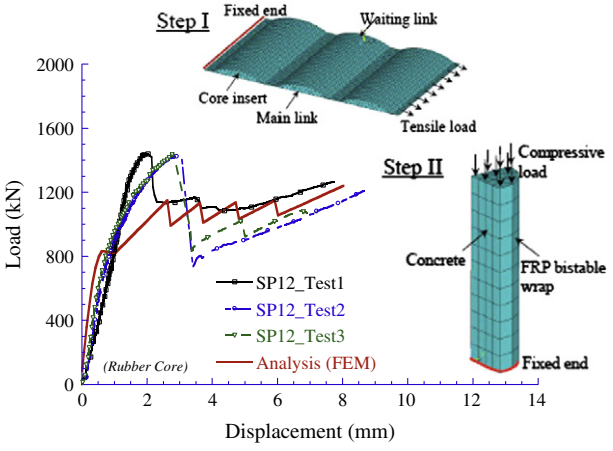

Fig. 8. Validation of the developed two-step modeling approach.

3.3. Validation using experimental data

To verify the developed model, test results from the bistable-confined concrete specimens with a 4-link 2%*wait* design using rubber cores were selected (three specimens included in the SP12-rubber set). The main link was made of one ply of CFRP and the waiting link had two plies of GFRP. Fig. 8 shows the load vs. axial displacement response of both the experimental and simulated confinement behavior. It can be seen that the simulation was able to capture the multi-stage loading mechanism (similar bistable trend to the material characterization tests). When the load reached the first peak, the first main link ruptured causing a small load drop. As the first waiting link has been activated, the load increased back again until the second main link fractured. This mechanism repeated several times until all main links failed and waiting links were activated. The load then continued to increase and reached the ultimate level when the waiting links ruptured. Although the first peak load from the simulation was lower than the experimental results, the ultimate load-carrying capacity (strength) of the confined concrete and the deformation (ductility) at failure were very close to what was obtained from the experiments. The proposed two-step simulation method provides a reasonable prediction in terms of overall bistable stress–strain behavior and deformability of FRP bistable-confined concrete.

4. Proposed stress–strain model for bistable-confined concrete

A number of theoretical strength models for conventional FRP-confined concrete exist in the open literature. The effectiveness of many of these models has also been demonstrated [4,9,10,26–32]. Since the FRP bistable-confined concrete behaves quite differently from the conventional case, these models will not be applicable to the bistable design discussed herein. Therefore, a new stress–strain constitutive model is specially derived and proposed in this study. As previously discussed, bistable structures could be made of a different number of bistable links. To demonstrate the idea of this new model, the 3-link bistable case is considered in the following derivation as an example. The same basic theory can be easily extended to derive the models for other cases such as 4-link or 5-link bistable structures.

4.1. Idealized bistable stress–strain model

To represent the multi-stage loading mechanism as observed in both test and numerical simulation, the bistable stress–strain curve is idealized by a multilinear curve, as illustrated in Fig. 9, which consists of five linear segments. For comparison purpose, the stress–strain curves for the unconfined concrete and traditional

FRP-confined concrete are also plotted in the same figure. f'_{co} and ε_{co} are the compressive strength and the corresponding axial strain of the unconfined concrete. Segments ① and ② intersect at the point where the compressive strain reaches ε_t. The slope of the first linear segment (Segment ①) corresponds to the equivalent initial Young's modulus in the confined concrete member (E_1). ε_{cc1}, ε_{cc2} and ε_{cc3} are the concrete strain when the first, second and third main link breaks, respectively. The peak stresses corresponding to these strain levels are represented by f'_{cc1}, f'_{cc2}, and f'_{cc3}, where $f'_{cc1} = f'_{cc2} = f'_{cc3}$. At the ultimate level, the concrete strain and strength before the waiting link fractures are denoted by ε_{cc4} and f'_{cc4}. It is further assumed that all the linear segments (Segments ②, ③, ④ and ⑤) except Segment ① would intersect at the same point on the vertical axis where the concrete strength is reduced to f'_{co} (i.e., $\sigma_c = f'_{co}$). This represents the unconfined concrete case when no FRP wrap or confinement exists and should be consistent for all design cases regardless of the number of bistable segments. The aforementioned design variables (E_1, f'_{cc1}, f'_{cc4}, ε_{cc1}, ε_{cc2}, ε_{cc3}, ε_{cc4}) need to be determined before the model can be established.

4.2. Model establishment via parametric study

In order to determine the above mentioned unknown design variables (E_1, f'_{cc1}, f'_{cc4}, ε_{cc1}, ε_{cc2}, ε_{cc3}, ε_{cc4}), a parametric study was conducted using the developed two-step finite element model as previously discussed. Important parameters that affect the bistable stress–strain behavior include the equivalent modulus and strength of the hybrid FRP bistable wrap (E_{frp}, f_{frp}), concrete compressive strength and modulus (f'_{co}, E_{co}), concrete member diameter (d), total confinement thickness (t_{frp}), and *%wait* in the bistable link design. The effect on the design variables due to these parameters is studied by conducting a series of separate analyses. Note that the equivalent modulus and strength of the hybrid FRP bistable wrap were extracted from the Step I modeling before they were used in Step II as the constitutive properties for the equivalent FRP wrap outside the concrete core. Fig. 10 graphically summarizes the results from such a parametric study (with a selected range of values for the parameters). Each parameter in the horizontal axis (such as E_{frp} and d) is normalized with respect to its corresponding initial value, and the undetermined design variables (such as f'_{cc1} and ε_{cc1}) are plotted in the vertical axis. Those initial values of the parameters are based on the ones used in the validated two-step modeling as previously discussed. The general trends observed from this study are concisely summarized below.

(1) *Equivalent FRP modulus* (E_{frp}) – The effect due to the equivalent FRP modulus is illustrated in Fig. 10a–c for concrete strengths (f'_{cc1}, f'_{cc4}), strain levels (ε_{cc1}, ε_{cc2}, ε_{cc3}, ε_{cc4}) and initial member modulus (E_1). It is evident that the equivalent modulus of the hybrid FRP bistable wrap has very little influence on the concrete strength (Fig. 10a). As the equivalent modulus increases, all concrete strains decrease nonlinearly (Fig. 10b) while the member's initial Young's modulus increases linearly (Fig. 10c).

(2) *Equivalent FRP strength* (f_{frp}) – Based on Fig. 10d–f, concrete strengths (f'_{cc1}, f'_{cc4}) and strains (ε_{cc1}, ε_{cc2}, ε_{cc3}, ε_{cc4}) show a linear increasing trend as the equivalent strength of the hybrid FRP bistable wrap increases (Fig. 10d and e); however, member's initial Young's modulus (E_1) is slightly independent of the FRP strength (Fig. 10f).

(3) *Concrete strength and modulus* (f'_{co} and E_{co}) – The unconfined concrete modulus is generally related to the concrete strength by $E_{co} = 4730\sqrt{f'_{\infty}}$ (MPa) per ACI 2005 [33]. Using this relation would essentially reduce the two variables to one independent design variable. Fig. 10g–i illustrates the effect due to the compressive strength of unconfined concrete (f'_{co}). It can be seen that both the confined concrete strengths (f'_{cc1}, f'_{cc4}) and the member's initial modulus (E_1) have a linear relationship with the unconfined concrete strength (f'_{co}), as clearly seen in Fig. 10g and i. This unconfined concrete strength has very little effect on the strain levels for bistable-confined concrete (ε_{cc1}, ε_{cc2}, ε_{cc3}, ε_{cc4}), as shown in Fig. 10h.

(4) *Concrete diameter* (d) – It is obvious from Fig. 10j that the confined concrete strengths (f'_{cc1}, f'_{cc4}) decrease nonlinearly with the increase of the concrete diameter (d). This similar trend applies to the member's initial modulus (E_1) as seen in Fig. 10l. However, the concrete strain levels (ε_{cc1}, ε_{cc2}, ε_{cc3}, ε_{cc4}) remain nearly constant (Fig. 10k).

(5) *Total confinement thickness* (t_{frp}) – As displayed in Fig. 10m and o, the confined concrete strengths (f'_{cc1}, f'_{cc4}) and the member's initial modulus (E_1) have a linear relationship with the FRP confinement thickness, while the strain levels (ε_{cc1}, ε_{cc2}, ε_{cc3}, ε_{cc4}) are independent of the total FRP thickness (Fig. 10n).

(6) *%wait* – The effect due to *%wait* in the bistable design is illustrated in Fig. 11. Referring to the same labels as used in Fig. 9, it is apparent that the confined concrete strength at the first peak (f'_{cc1}) and member's initial modulus (E_1) decrease slightly as the *%wait* increases from 2% to 9%. The strain levels (ε_{cc2}, ε_{cc3}, ε_{cc4}), on the other hand, increase dramatically. This can be explained by the fact that the larger the *%wait* is, the later the waiting links are activated, therefore the larger the deformation reaches in the structure. The ultimate concrete strength (f'_{cc4}) and the strain at the first peak (ε_{cc1}) show very little change as the *%wait* increases.

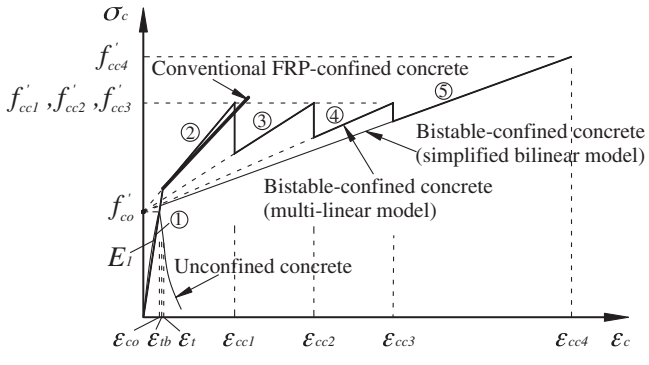

Fig. 9. Idealized description for bistable stress–strain model.

4.3. Proposed bistable stress–strain model

Based on the results acquired from the parametric study, a typical nonlinear data fitting process was performed next in order to formulate the desired variables (f'_{cc1}, f'_{cc4}, ε_{cc1}, ε_{cc2}, ε_{cc3}, ε_{cc4} and E_1) in terms of the key parameters (E_{frp}, f_{frp}, f'_{co}, E_{co}, d, t_{frp} and *%wait*). Since the equivalent modulus and strength of the FRP bistable wrap (E_{frp}, f_{frp}) are linked to the material properties of the individual layers (CFRP and GFRP), the strength, modulus and thickness of the raw CFRP and GFRP layers are directly used in the derivations from this point on. The formulas thus derived can be described below, which share the similar basic format in the strength model as reported in Ref. [9]:

$$f'_{cc1} = f'_{cc2} = f'_{cc3} = f'_{\infty} + 0.88\frac{2f_{cfrp}t_{cfrp}}{d}\,(\%wait)^{-0.3} \tag{1}$$

$$f'_{cc4} = f'_{co} + 2.05\frac{2f_{gfrp}t_{gfrp}}{d} \tag{2}$$

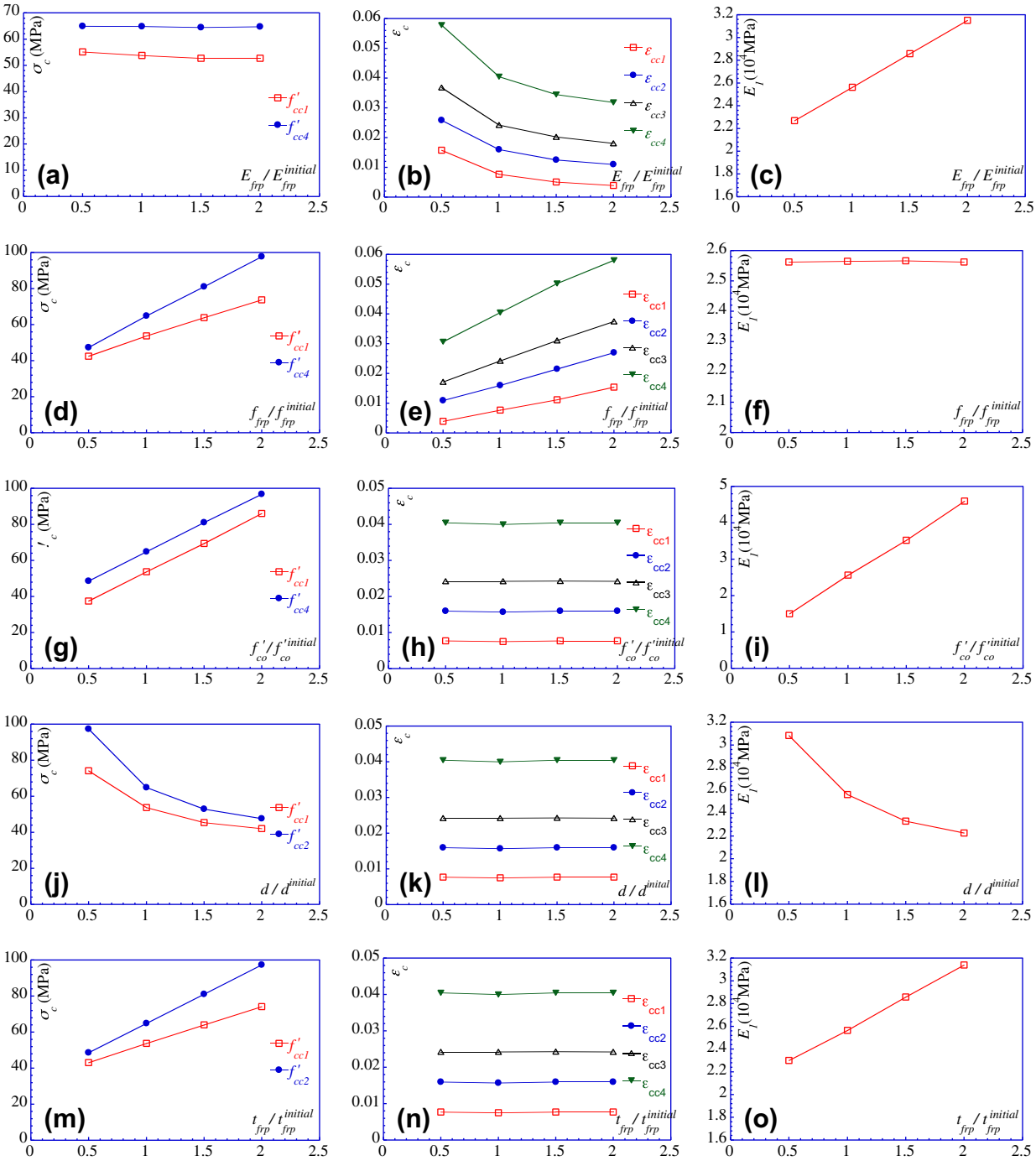

Fig. 10. Parametric study on effect due to: (a–c) FRP modulus, (d–f) FRP strength, (g–i) concrete strength, (j–l) member diameter and (m–o) confinement thickness.

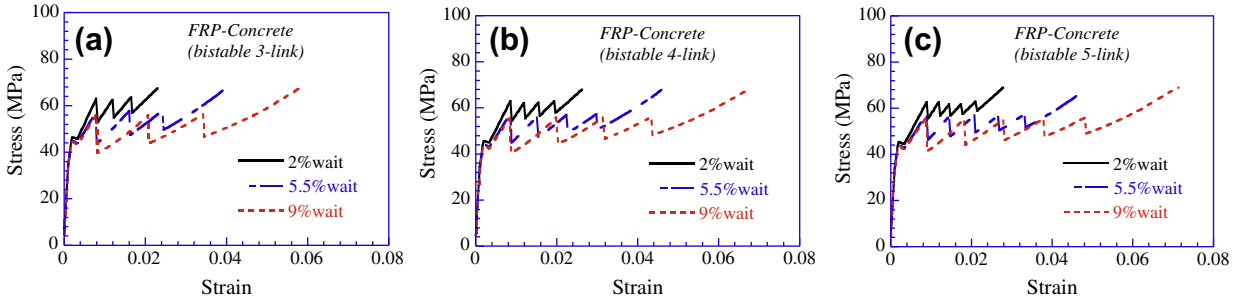

Fig. 11. Parametric study on effect due to *%wait* for design with: (a) 3-link, (b) 4-link and (c) 5-link.

$$\varepsilon_{cc1} = \varepsilon_{co} + 2.54\left(\frac{f_{cfrp}}{E_{cfrp}\varepsilon_{co}}\right)^{1.4}\varepsilon_{co}\ (\%wait)^{0.8} \tag{3}$$

$$\varepsilon_{cc2} = \varepsilon_{cc1} + 29.52\left(\frac{f_{cfrp}}{E_{cfrp}\varepsilon_{co}}\right)^{0.2}\varepsilon_{co}\ (\%wait)^{0.8} \tag{4}$$

$$\varepsilon_{cc3} = \varepsilon_{cc2} + 29.52\left(\frac{f_{cfrp}}{E_{cfrp}\varepsilon_{co}}\right)^{0.2}\varepsilon_{co}\ (\%wait)^{0.8} \tag{5}$$

$$\varepsilon_{cc4} = \varepsilon_{cc3} + 50.9\left(\frac{f_{cfrp}}{E_{cfrp}\varepsilon_{co}}\right)^{0.2}\varepsilon_{co}\ (\%wait)^{0.8} \tag{6}$$

$$E_1 = 538.9f'_{\infty} + 8.17\frac{2E_{cfrp}t_{cfrp}}{d} \tag{7}$$

where f_{cfrp}, E_{cfrp} and t_{cfrp} are the tensile strength, elastic modulus and thickness of the CFRP layer, respectively, and the values such as 0.88 and −0.3 are the curve fitting coefficients. Similarly, f_{gfrp}, E_{gfrp} and t_{gfrp} are the properties of the GFRP layers. ε_{co} is the axial strain of the unconfined concrete at its peak stress that has a typical value of 0.002. Using these strength and strain levels depicted by Eqs. (1)–(7), a piecewise function is then derived below to describe the proposed multilinear stress–strain response for the FRP bistable-confined concrete (as illustrated in Fig. 9):

$$\sigma_c = \begin{cases} E_1\varepsilon_c & , \quad 0 \leqslant \varepsilon_c < \varepsilon_t \\ f'_{co} + \frac{f'_{cc1}-f'_{co}}{\varepsilon_{cc1}}\varepsilon_c & , \quad \varepsilon_t \leqslant \varepsilon_c < \varepsilon_{cc1} \\ f'_{co} + \frac{f'_{cc2}-f'_{co}}{\varepsilon_{cc2}}\varepsilon_c & , \quad \varepsilon_{cc1} \leqslant \varepsilon_c < \varepsilon_{cc2} \\ f'_{co} + \frac{f'_{cc3}-f'_{co}}{\varepsilon_{cc3}}\varepsilon_c & , \quad \varepsilon_{cc2} \leqslant \varepsilon_c < \varepsilon_{cc2} \\ f'_{co} + \frac{f'_{cc4}-f'_{co}}{\varepsilon_{cc4}}\varepsilon_c & , \quad \varepsilon_{cc3} \leqslant \varepsilon_c > \varepsilon_{cc4} \end{cases} \tag{8}$$

where σ_c and ε_c are the axial stress and strain of the bistable-confined concrete under compression. ε_t is the so-called transition strain, meaning the strain of the intersection of linear Segments ① and ② (as labeled in Fig. 9), which is given by:

$$\varepsilon_t = \frac{f'_{co}}{E_1 - \frac{f'_{cc1}-f'_{co}}{\varepsilon_{cc1}}} \tag{9}$$

4.4. Simplified bilinear stress–strain model and accuracy verification

Although straightforward, the multilinear stress–strain model could be tedious to apply especially for design purpose. To further simplify it, a bilinear stress–strain curve is proposed here, as illustrated in Fig. 9, where the intermediate linear segments are simply replaced by a lower bound linear segment extended from Segment ⑤ for a conservative estimate. Correspondingly, the stress function can be formulated by the following equation:

$$\sigma_c = \begin{cases} E_1\varepsilon_c & , \quad 0 \leqslant \varepsilon_c < \varepsilon_{tb} \\ f'_{co} + \frac{f'_{cc4}-f'_{co}}{\varepsilon_{cc4}}\varepsilon_c & , \quad \varepsilon_{tb} \leqslant \varepsilon_c < \varepsilon_{cc4} \end{cases} \tag{10}$$

where ε_{tb} is the transition strain from linear segment ① to linear segment ⑤ (see Fig. 9), which is given by Eq. (11) below. Other parameters such as f'_{cc4}, ε_{cc4} and E_1 can be calculated from Eqs. (2), (6), and (7), respectively.

$$\varepsilon_{tb} = \frac{f'_{co}}{E_1 - \frac{f'_{cc4}-f'_{co}}{\varepsilon_{cc4}}} \tag{11}$$

To verify the accuracy of this simplified stress–strain model for bistable-confined concrete, a set of twenty-three design cases was selected from the sample pool in the parametric study. It includes four cases in each category of FRP modulus, FRP strength, concrete strength, concrete diameter and confinement thickness, and three cases in the *%wait* category. The verification was performed on the same design variables including f'_{cc1}, f'_{cc4}, ε_{cc1}, ε_{cc2}, ε_{cc3}, ε_{cc4} and E_1. Fig. 12 shows the distribution of the percentage ratio of the results obtained from the analysis using the proposed simplified stress–strain model and the simulation using the multilinear stress–strain model (Fig. 12a is for variables f'_{cc1} and f'_{cc4}; Fig. 12b for ε_{cc1}, ε_{cc2}, ε_{cc3}, ε_{cc4}; and Fig. 12c for E_1). Statistical results such as average ratio (Avg.), standard deviation ratio (SD) and coefficient of variation ratio (COV) of each variable are also shown in the same plots. It can be seen that the proposed simplified bilinear model can reproduce the results from the simulated multilinear model with good accuracy (average percentage ratios close to 100%). The coefficient of variation for all variables is no larger than 4%, indicating an extremely low level of dispersion.

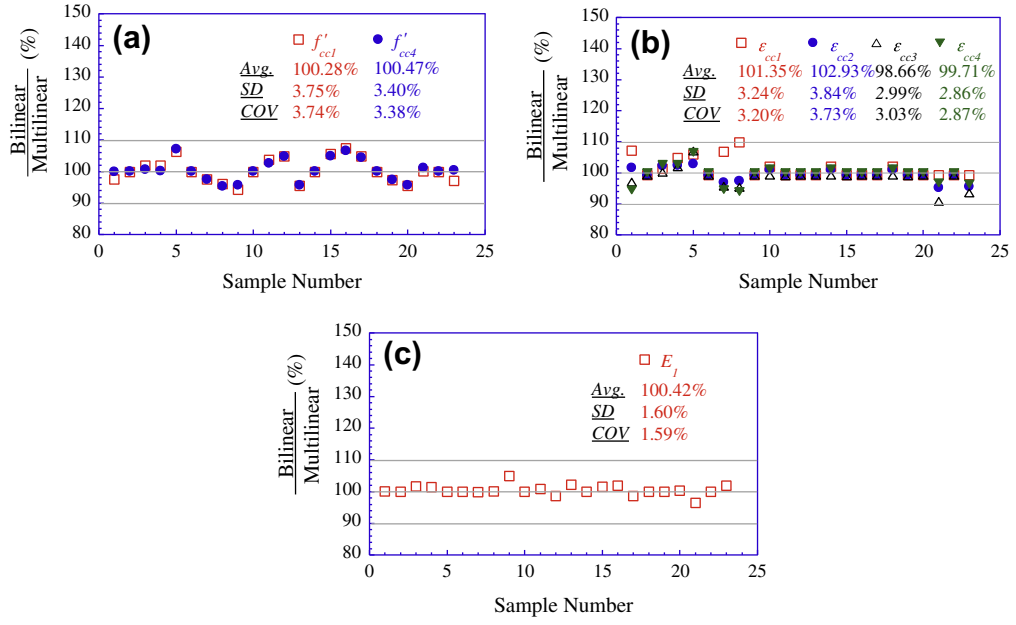

Fig. 12. Comparison of the proposed simplified bilinear and simulated multilinear stress–strain models for: (a) concrete strength, (b) strain levels and (c) member modulus.

5. Conclusions

The use of mechanism-based hybrid FRP bistable wrap for concrete confinement is investigated in this study. The hybrid FRP bistable structures consist of energy-absorbing "links" made of carbon and glass FRP with the main links designed as the primary load carrier and the waiting links as the secondary load carrier. Several parameters were studied, including the type of FRP reinforcement, amount of stitching, material type of inserting core (foam, wood, rubber vs. aluminum) and alternative wrapping methods. A two-step simulation method is developed where a theoretical bistable stress–strain model was proposed based on analytical derivation and experimental data. This approach offers a conceptual framework viable for modeling concrete confinement. The following conclusions are drawn based on the current study:

1. The FRP bistable-confined concrete was found to have an increased ductility and energy absorption with a safer and controlled pseudo-ductile failure mode. This could be advantageous in seismic retrofit of reinforced concrete columns such as in the plastic hinge regions where large inelastic deformation is desired.
2. Stitching tends to stiffen the local area of FRP wrap and was found to contribute to early debonding in the structure. Therefore, a minimum amount of stitching should be used.
3. The multi-stage bistable behavior is best achieved in the design using CFRP for main link and GFRP for waiting link, which also provides the greatest amount of energy absorption compared to the use of GFRP for the main links and CFRP for the waiting links.
4. The alternative manufacturing process using a layer-by-layer method significantly increased the load-carrying capacity of the specimens as compared with the original method.
5. Among the different types of core inserts studied (foam, wood, rubber and aluminum), rubber provided the desirable amount of deformability and energy absorption in the bistable-confined concrete, thus reducing the tendency for brittle failure. Rubber core inserts remained in one piece whereas foam or wood core inserts experienced fragmentation. Rubber thus provides a good candidate for the core inserts of the bistable structure.
6. The proposed two-step simulation method provides an accurate prediction in terms of the overall bistable stress–strain behavior and deformability of FRP bistable-confined concrete. The simplified bilinear stress–strain model is suitable for practical design purposes with acceptable precision.

Other relevant parameters, including the radius of the insert and alternative FRP reinforcement such as spectrum, could be investigated in a future study. More advanced stress–strain models can be further considered to better characterize the behavior of concrete confined by FRP bistable structures.

Acknowledgements

The writers wish to acknowledge the financial support provided by the Hellman Foundation Board to the second author on this research (2008–2009 UC Davis Hellman Fellows) and the Chinese Scholarship Council to the third author during his visit at the University of California, Davis.

References

[1] Fardis M, Khalili H. Concrete encased in fiberglass reinforced plastic. ACI J 1981;78(6):440–6.
[2] Saadatmanesh H, Ehsani M, Li M. Strength and ductility of concrete columns externally reinforced with fiber composite straps. ACI Struct J 1994;91(4):434–47.
[3] Seible F, Priestley MJ, Hegemier G, Innamorato D. Seismic retrofit of RC concrete columns with continuous carbon fiber jacket. ASCE J Compos Constr 1997;1(2):52–62.
[4] Xiao Y, Wu H. Compressive behavior of concrete confined by carbon fiber composite jackets. ASCE J Mater Civ Eng 2000;12(2):139–46.
[5] Lam L, Teng JG, Cheung C, Xiao Y. FRP-confined concrete under axial cyclic compression. Cem Concr Compos 2006;28(10):949–58.
[6] Ozbakkaloglu T, Saatcioglu M. Seismic performance of square high-strength concrete columns in FRP stay-in-place formwork. ASCE J Struct Eng 2007;133(1):44–56.
[7] Li J, Hadi M. Behavior of externally confined high-strength concrete columns under eccentric loading. Compos Struct 2003;62(2):145–53.
[8] Quiertant M, Clement JL. Behavior of RC columns strengthened with different CFRP systems under eccentric loading. Constr Build Mater 2011;25(2):452–60.
[9] Karbhari VM, Gao Y. Composite jacketed concrete under uniaxial compression-verification of simple design equations. ASCE J Mater Civ Eng 1997;9(4):185–93.
[10] Samaan M, Mirmiran A, Shahawy M. Model of concrete confined by fiber composites. ASCE J Struct Eng 1998;124(9):1025–31.
[11] Spoelstra M, Monti G. FRP-confined concrete model. ASCE J Compos Constr 1999;3(3):143–50.
[12] Teng JG, Lam L. Behavior and modeling of fiber reinforced polymer-confined concrete. ASCE J Struct Eng 2004;130(11):1713–23.
[13] Realfonzo R, Napoli A. Concrete confined by FRP systems: confinement efficiency and design strength models. Compos B Eng 2011;42(4):736–55.
[14] Karantzikis M, Papanicolaou C, Antonopoulos C, Triantafillou T. Experimental investigation of nonconventional confinement for concrete using FRP. ASCE J Compos Constr 2005;9(6):480–7.
[15] Park TW, Na UJ, Chung L, Feng M. Compressive behavior of concrete cylinders confined by narrow strips of CFRP with spacing. Compos B Eng 2008;39(7–8):1093–103.
[16] Anggawidjaja D, Ueda T, Dai J, Nakai H. Deformation capacity of RC piers wrapped by new fiber-reinforced polymer with large fracture strain. Cem Concr Compos 2006;28(10):914–27.
[17] Matthys S, Taerwe L. Evaluation of ductility requirements in current design guidelines for FRP strengthening. Cem Concr Compos 2006;28(10):845–56.
[18] Cherkaev A, Slepyan L. Waiting element structures and stability under extension. Int J Damage Mech 1995;4(1):58–82.
[19] Winkelmann C, Kim S, La Saponara V. Design and development of hybrid composite bistable structures for energy absorption under quasi-static loading. Compos Struct 2010;93(1):171–8.
[20] Wan C, Quon C, Cheng L. Mechanism-based composite structure and its application in concrete column retrofit. In: Proceedings of SAMPE, Baltimore, MD; 2009.
[21] Wan C, Cheng L, Quon C, Li Y. Compressive behavior of concrete confined by a mechanism-based fiber composite bistable structure. ASCE J Mater Civ Eng 2011;23(12):1755–9.
[22] ASTM D3039/D3039M. Standard test method for tensile properties of polymer matrix composite materials. West Conshohocken (PA): ASTM International; 2005.
[23] ASTM C39/C39M. Standard test method for compressive strength of cylindrical concrete specimens. West Conshohocken (PA): ASTM International; 2005.
[24] ANSYS. Computational dynamics North America Ltd., Version 10.0. 2005.
[25] Hognestad E. A study of combined bending and axial load in reinforced concrete members. Bulletin series no. 399. Engineering experiment station, III. Urbana: Univ. of Illinois; 1951.
[26] Miyauchi K, Inoue S, Kuroda T, Kobayashi A. Strengthening effects with carbon fiber sheet for concrete column. Proc Jpn Concr Inst 1999;21(3):1453–8. in Japanese.
[27] Saafi M, Toutanji HA, Li Z. Behavior of concrete columns confined with fiber reinforced polymer tubes. ACI Mater J 1999;96(4):500–9.
[28] Toutanji HA. Stress–strain characteristics of concrete columns externally confined with advanced fiber composite sheets. ACI Mater J 1999;96(3):397–404.
[29] Lam L, Teng JG. Strength models for fiber-reinforced plastic confined concrete. ASCE J Struct Eng 2002;128(5):612–23.
[30] Lam L, Teng JG. Design-oriented stress–strain model for FRP-confined concrete. Constr Build Mater 2003;17(6–7):471–89.
[31] Ilki A, Peker O, Karamuk E, Demir C, Kumbasar N. FRP retrofit of low and medium strength circular and rectangular reinforced concrete columns. ASCE J Mater Civ Eng 2008;20(2):169–88.
[32] Lee CS, Hegemier GA. Model of FRP-confined concrete cylinders in axial compression. ASCE J Compos Constr 2009;13(5):442–54.
[33] ACI 318-05. Building code requirements for structural concrete and commentary. Michigan: American Concrete Institute (ACI Committee 318); 2005.